Modelling the development and decay of cryoconite holes in Northwest Greenland

Yukihiko Onuma[1], Koji Fujita[2], Nozomu Takeuchi[3], Masashi Niwano[4] and Teruo Aoki[5]

[1]Earth Observation Research Center (EORC), Japan Aerospace Exploration Agency (JAXA), Tsukuba, 305-8505, Japan
[2]Graduate School of Environmental Studies, Nagoya University, Nagoya 464-8601, Japan
[3]Graduate School of Science, Chiba University, Chiba 263-8522, Japan
[4]Meteorological Research Institute, Japan Meteorological Agency, Tsukuba 305-0052, Japan
[5]National Institute of Polar Research, Tokyo 190-8518, Japan

Correspondence to: Yukihiko Onuma[1] and Koji Fujita[2] ([1]onuma.yukihiko@jaxa.jp and [2]cozy@nagoya-u.jp)

SUPPLEMENTARY MATERIAL

S1. Broadband flux extinction coefficient of bare ice

S1.1 Theoretical basis

This supplementary section presents an expression for the broadband asymptotic volume flux extinction coefficient, for which the term κ (m^{-1}) is used in Sect. 2.4, from the spectral asymptotic volume flux extinction coefficient $k_e(\lambda)$ (m^{-1}) of bare ice, where λ is the wavelength (μm). In this study, we simply refer to them as the "broadband (or spectral) flux extinction coefficient." When the bare ice surface is illuminated by the spectral solar radiation $F_s(\lambda)$, the attenuated solar radiation $F_b(\lambda)$ at ice thickness x in bare ice is expressed by $k_e(\lambda)$ as follows:

$$F_b(\lambda) = F_s(\lambda)\exp\left[-k_e(\lambda)x\right]. \quad \text{(S1)}$$

Using Eq. (S1), the spectral flux transmittance ($T(\lambda, x)$; dimensionless) as a function of x is described as follows:

$$T(\lambda, x)=\frac{F_b(\lambda)}{F_s(\lambda)} = \exp\left[-k_e(\lambda)x\right]. \quad \text{(S2)}$$

The spectrally integrated flux transmittance $\bar{T}(x)$ is calculated from $F_s(\lambda)$ and $T(\lambda, x)$ as follows:

$$\bar{T}(x) = \frac{\int_0^\infty F_s(\lambda)T(\lambda,x)d\lambda}{\int_0^\infty F_s(\lambda)d\lambda}. \quad \text{(S3)}$$

Using Eq. (S3), the broadband flux extinction coefficient ($\overline{k_e}(x)$, m^{-1}) is described as follows:

$$\overline{k_e}(x) = \frac{-ln\left(\bar{T}(x)\right)}{x} = -ln\left(\frac{\int_0^\infty F_s(\lambda)\exp\left[-k_e(\lambda)x\right]d\lambda}{\int_0^\infty F_s(\lambda)d\lambda}\right)/x. \quad \text{(S4)}$$

S1.2 Parameterization of $\overline{k_e}(x)$ for clear and cloudy sky conditions

Using Eq. (S4), we calculate the $\overline{k_e}(x)$ for bare ice in Greenland from the following two datasets for $k_e(\lambda)$ and $F_s(\lambda)$. The first data set $k_e(\lambda)$ is employed based on the measurements by Cooper et al. (2021) for the bare ice "Layer A" and "Layer B," which are defined as the ice layers from 12 to 77 cm depth and 53 to 124 cm depth, respectively. The second dataset $F_s(\lambda)$ is theoretically simulated at $\lambda = 0.2 - 4.0$ μm with a spectral resolution of 0.025 μm using a radiative transfer model for the atmosphere–snow/ice system (Aoki et al., 1999; 2000), assuming clear and cloudy sky conditions in the subarctic model atmosphere over the bare ice surface. Since the spectral range of $k_e(\lambda)$ reported by Cooper et al. (2021) is limited around the visible wavelengths ($\lambda = 0.35 - 0.75$μm), with their Table A1 data ($\lambda = 0.35 - 0.60$μm) and the calculated values from their transmittance data ($\lambda = 0.60 - 0.75$μm) being employed in this study, we assume $k_e(\lambda)$ in the other spectral regions $\lambda = 0.2 - 0.35$ μm and $\lambda = 0.75 - 4.0$ μm by scaling the spectral absorption coefficient $k_a(\lambda)$ of pure ice (Warren and Brandt, 2008) to connect to the values of Cooper et al. (2021), as shown in Figure S1. It is inferred that the difference between the scaled $k_e(\lambda)$ (pink curve) and $k_a(\lambda)$ for pure ice (blue curve and red "x" symbols) is attributed to air bubbles in bare ice for $\lambda \geq 0.55$ μm, and impurities and air bubbles for $\lambda < 0.55$ μm from the discussion by Cooper et al. (2021). There are large uncertainties in $k_a(\lambda)$ in $\lambda = 0.35 - 0.75$ μm, as shown by the blue curve (Warren and Brandt, 2008) and the red "x" symbols (Cooper et al., 2021) in Figure S1. Regarding the validity of the scaled $k_e(\lambda)$ in other spectral regions, we did not have verifiable data. In fact, the contribution to $\overline{k_e}(x)$ from $k_e(\lambda)$ in the other spectral regions is very low. The simulated $F_s(\lambda)$ for clear and cloudy skies in the case of the solar zenith angle $\theta_z = 63.1°$ is shown in Figure S2.

Figure S3 demonstrates $\overline{k_e}(x)$ as a function of θ_z in the case of $x = 0.1$ m calculated from $k_e(\lambda)$ and $F_s(\lambda)$ described above using Eq. (S4). There is almost no difference in $\overline{k_e}(x)$ when we use $k_e(\lambda)$ for Layer A and Layer B, as observed by Cooper et al. (2021). We also find that the θ_z dependence of $\overline{k_e}(x)$ is small in the range of θ_z from 50 to 86°, and thus, we determine the θ_z-independent values of $\overline{k_e}(x)$ by averaging it over this range of θ_z. By plotting the θ_z-independent values of $\overline{k_e}(x)$ as a function of x for clear and cloudy skies (Fig. S4), the values of $\overline{k_e}(x)$ rapidly decrease in the shallower ice layer and change to a gentle slope in the deeper ice layer when x increases. This is because the spectral distribution of $F_b(\lambda)$ in bare ice changes from a wider distribution to a narrower distribution centred around the wavelength of the minimum $k_e(\lambda)$, where the light absorption by bare ice is weakest as the x increases. We can then obtain the approximation equations by fitting the calculated values of $\overline{k_e}(x)$ with a power regression equation, as shown in Table S1. In this study, we use the terms "κ_{clr}" and "κ_{cld}" as

the values of $\overline{k_e}(x)$ for clear and cloudy skies, respectively. κ_{clr} and κ_{cld} are calculated using the values of Layer A shown in Table S1, because we focus on the vertical change of cryoconite holes below 20 cm (Eqs (22) and (23) in the main manuscript). Finally, the broadband flux extinction coefficient for the diffuse component (κ_f) is determined using the diffuse ratio of the downward shortwave radiation based on the solar zenith angle and cloudiness (Eq. (24)).

References

Aoki, T., Aoki, T., Fukabori, M., Hachikubo, A., Tachibana, Y., and Nishio, F.: Effects of snow physical parameters on spectral albedo and bidirectional reflectance of snow surface, J. Geophys. Res., 105, 10219–10236. https://doi.org/10.1029/1999JD901122, 2000.

Aoki, T., Aoki, T., Fukabori, M., and Uchiyama, A.: Numerical simulation of the atmospheric effects on snow albedo with a multiple scattering radiative transfer model for the atmosphere-snow system, J. Meteorol. Soc. Jpn, 77, 595–614. https://doi.org/10.2151/jmsj1965.77.2_595, 1999.

Cooper, M. G., Smith, L. C., Rennermalm, A. K., Tedesco, M., Muthyala, R., Leidman, S. Z., Moustafa, S. E., and Fayne, J. V.: Spectral attenuation coefficients from measurements of light transmission in bare ice on the Greenland Ice Sheet, Cryosphere, 15, 1931–1953. https://doi.org/10.5194/tc-15-1931-2021, 2021.

Warren, S. G. and Brandt, R. E.: Optical constants of ice from the ultraviolet to the microwave: A revised compilation, J. Geophys. Res., 113. https://doi.org/10.1029/2007JD009744, 2008.

Table S1: Approximation equation parameters fitted by a power regression equation $\overline{k_e}(x) = ax^b$ for clear and cloudy sky conditions and employed data sets of $k_e(\lambda)$ for Layer A and Layer B reported by Cooper et al. (2021). R^2 is the determination coefficient.

Sky condition	Ice layer	*a*	*b*	R^2
Clear sky	Layer-A	1.9167	-0.61328	0.995
Cloudy sky	Layer-A	1.6203	-0.51923	0.991
Clear sky	Layer-B	1.8322	-0.62486	0.996
Cloudy sky	Layer-B	1.529	-0.53297	0.993

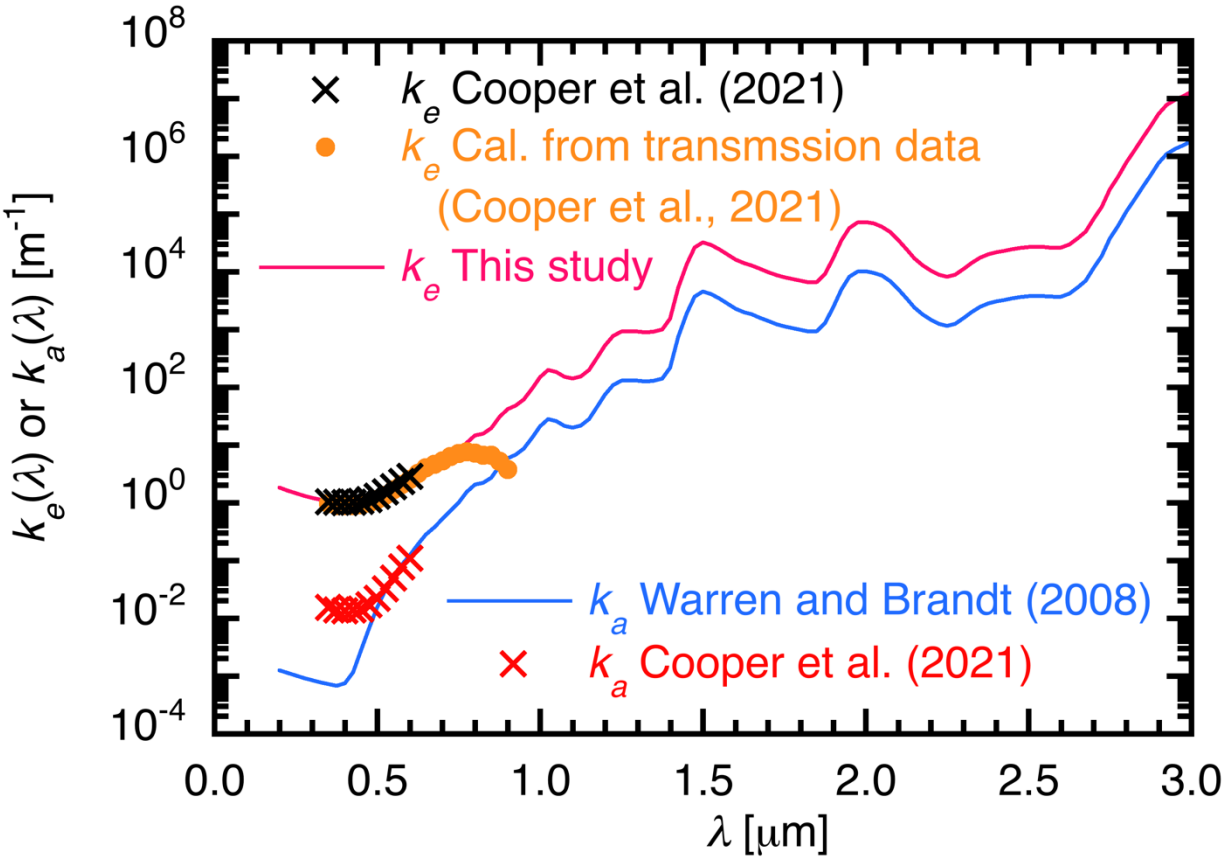

Figure S1: Spectral flux extinction coefficient ($k_e(\lambda)$) and absorption coefficient ($k_a(\lambda)$) in $\lambda = 0.2 - 3.0$ μm used for the calculation of $\overline{k_e}(x)$. $k_e(\lambda)$ data for the wider spectral region in $\lambda = 0.2 - 4.0$ μm are used in the calculation of $\overline{k_e}(x)$. Green "x" symbols are $k_e(\lambda)$ reported by Cooper et al. (2021) for Layer A, orange dots are $k_e(\lambda)$ calculated from the transmittance data observed by Cooper et al. (2021), pink curve is $k_e(\lambda)$ used in this study, blue curve is $k_a(\lambda)$) calculated from imaginary refractive index of pure ice (Warren and Brandt, 2008), and red "x" symbols are $k_a(\lambda)$ shown in Figure S1 of Cooper et al. (2021) for Layer A, which is just a reference for comparison with $k_a(\lambda)$ of Warren and Brandt (2008).

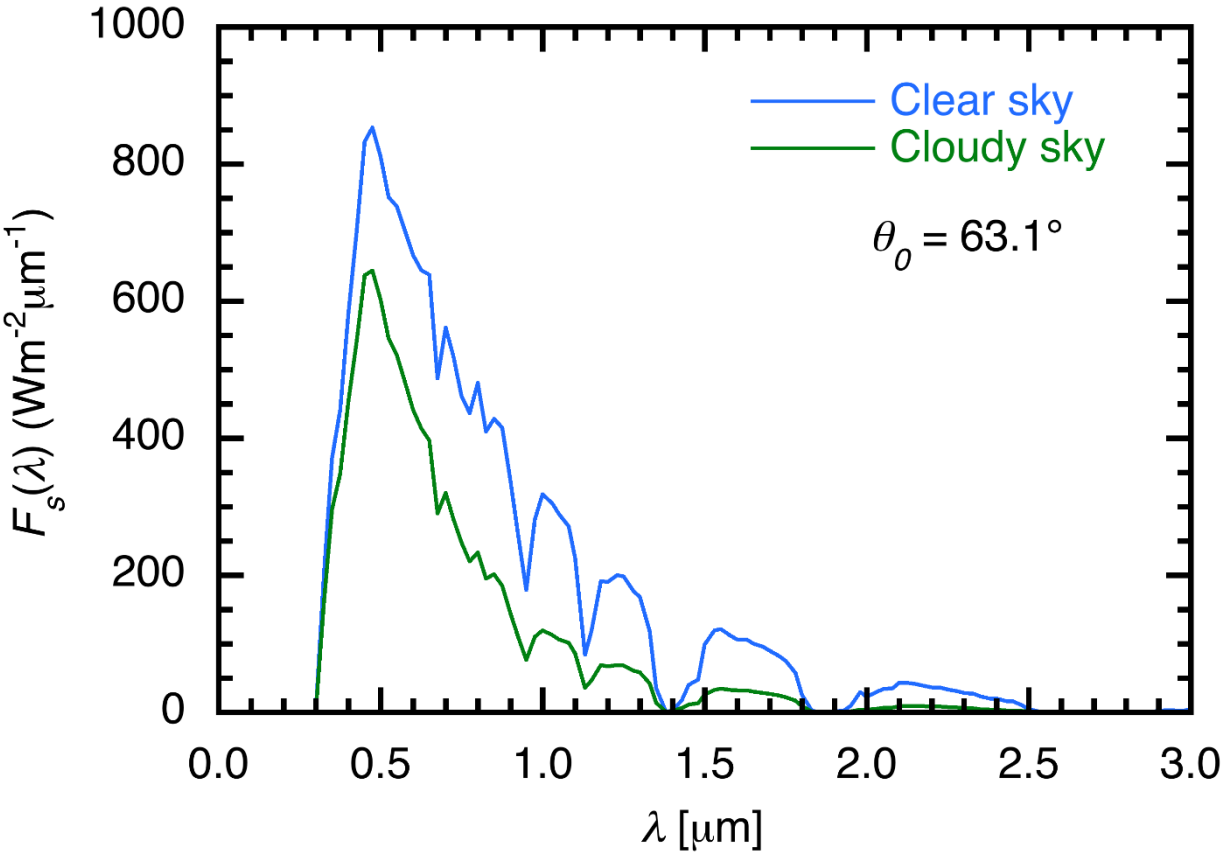

Figure S2: Spectral solar radiation $F_s(\lambda)$ in $\lambda = 0.2 - 3.0$ μm under clear and cloudy skies at $\theta_0 = 63.1°$, simulated with a radiative transfer model for the atmosphere–snow/ice system over the bare ice surface with a spectral resolution of 0.025 μm. In the calculation of $\overline{k_e}(x)$, $F_s(\lambda)$ in $\lambda = 0.2 - 4.0$ μm is used.

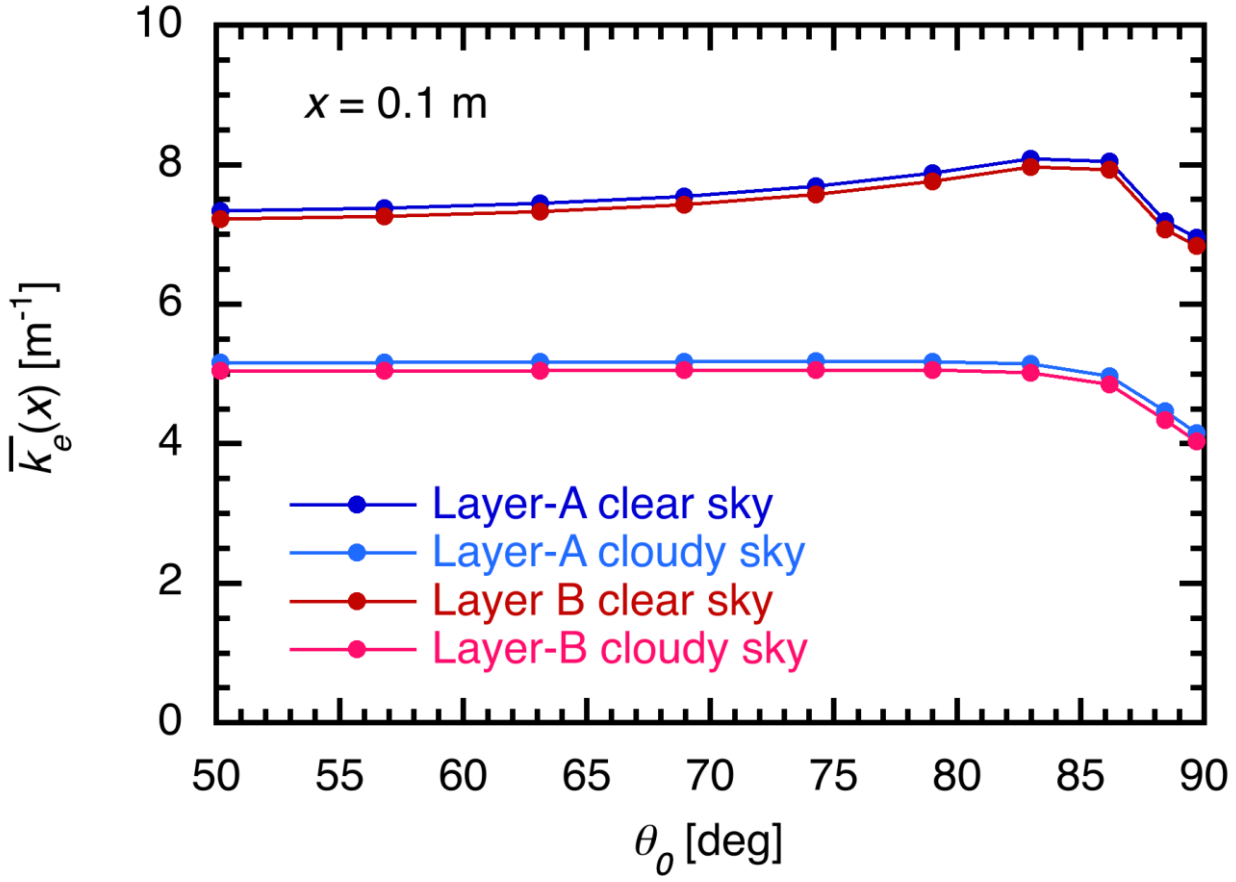

Figure S3: Broadband flux extinction coefficient $\overline{k_e}(x)$ of bare ice as a function of θ_0 in the case of $x = 0.1$ m for clear and cloudy sky conditions and employed data sets of $k_e(\lambda)$ for Layer A and Layer B reported by Cooper et al. (2021).

95

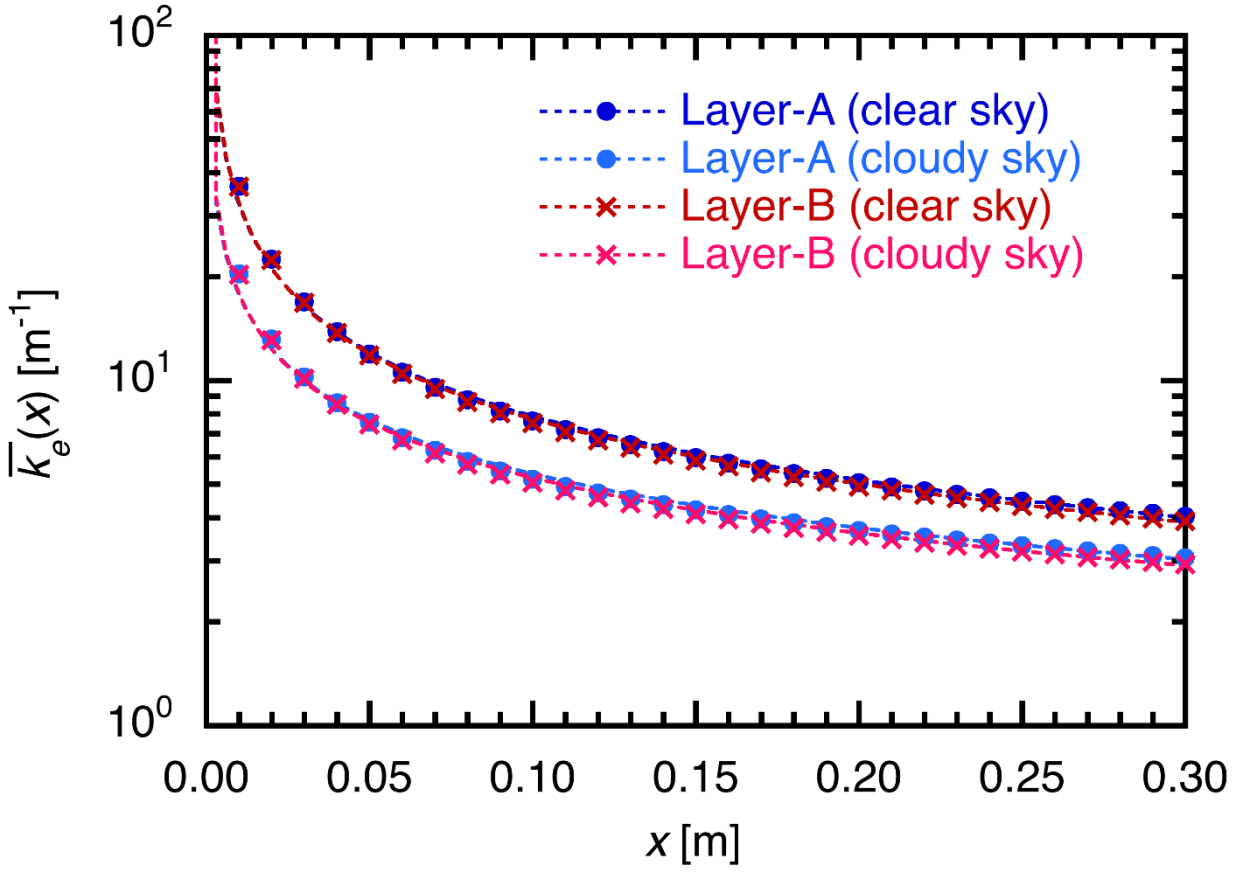

Figure S4: Broadband flux extinction coefficient $\overline{k_e}(x)$ of bare ice as a function of ice thickness x for clear and cloudy sky conditions and employed data sets of $k_e(\lambda)$ for Layer A and Layer B reported by Cooper et al. (2021). Calculated values are indicated by symbols and dashed curves are approximation equations fitted by power regression equations.

100

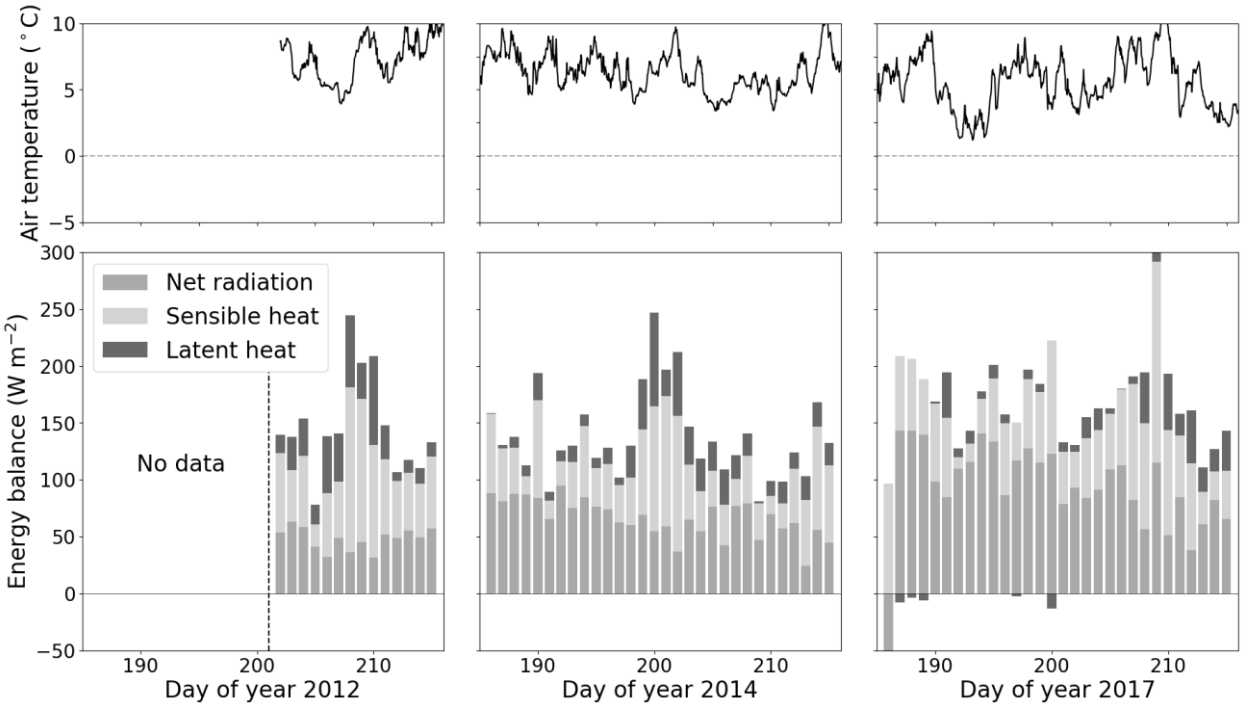

Figure S5: Hourly air temperature (upper panels) and daily surface energy balance (lower panels) at Site 2 on the Qaanaaq ice cap during the 2012, 2014, and 2017 summer seasons from left to right, respectively. Air temperature at Site 2 is corrected based on the data obtained by an automatic weather station at Site 5 and an observed lapse rate (see main article). Daily surface energy balance is calculated with CryHo.

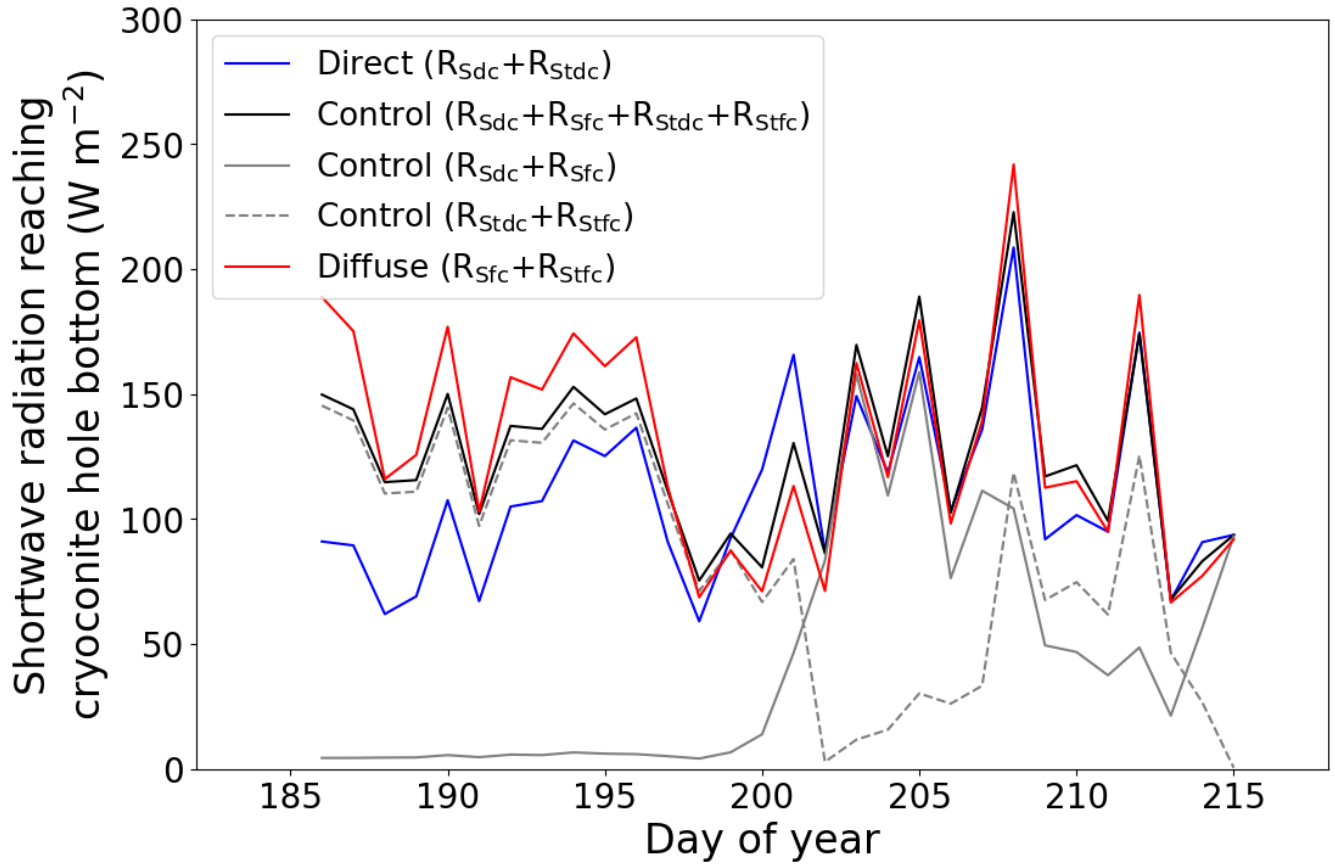

Figure S6: Daily mean temporal changes in direct and diffuse components of shortwave radiation reaching the cryoconite hole (CH) bottom in 2014. Blue and red lines indicate the direct (R_{sdt}+R_{stdc}) and diffuse (R_{sfct}+R_{stfc}) components in R_S-exp, respectively. Black line indicates both component of shortwave radiation (R_{sdt}+ R_{sfct}+ R_{stdc}+R_{stfc}) in Ctl-exp. Grey solid and dashed lines indicate the radiation components reaching the CH bottom from the hole mouth (R_{sdt}+ R_{stdc}) and transmitting through ice (R_{sfct}+ R_{stfc}) in Ctl-exp, respectively.